Langmuir
Article
pubs.acs.org/Langmuir

Attraction between Particles at a Liquid Interface Due to the Interplay of Gravity- and Electric-Field-Induced Interfacial Deformations

Mariana P. Boneva, Krassimir D. Danov, Nikolay C. Christov, and Peter A. Kralchevsky*

Laboratory of Chemical Physics & Engineering, Faculty of Chemistry, Sofia University, 1164 Sofia, Bulgaria

Received February 26, 2009. Revised Manuscript Received April 25, 2009

In a previous study, we established that the attraction between electrically charged particles attached to a water/tetradecane interface is stronger than predicted on the basis of the gravity-induced lateral capillary force. Here, our goal is to explain this effect. The investigated particles are hydrophobized glass spheres of radii between 240 and 320 μm. Their weight is large enough to deform the liquid interface. The interfacial deformation is considerably greater for charged particles because of the electrodipping force that pushes the particles toward the water phase. By independent experiments with particles placed between two electrodes, we confirmed the presence of electric charges at the particle/tetradecane interface. The theoretical analysis shows that if the distribution of these surface charges is isotropic, the meniscus produced by the particle electric field decays too fast with distance and cannot explain the experimental observations. However, if the surface-charge distribution is anisotropic, it induces a saddle-shaped deformation in the liquid interface around each particle. This deformation, which is equivalent to a capillary quadrupole, decays relatively slow. Its interference with the gravity-induced isotropic meniscus around the other particle gives rise to a long-range attractive capillary force, $F \sim 1/L^3$ (L = interparticle distance). The obtained agreement between the experimental and theoretical curves, and the reasonable values of the parameters determined from the fits, indicate that the observed stronger attraction in the investigated system can be really explained as a hybrid interaction between gravity-induced "capillary charges" and electric-field-induced "capillary quadrupoles".

1. Introduction

Liquid interfaces can serve as templates for self-assembly and ordering of various colloidal particles.[1−3] The ordering process and the obtained structures are influenced by the acting interparticle forces.[4,5] For example, in the presence of electrostatic repulsion between like-charged colloidal particles, nondensely packed interfacial colloidal crystals are formed,[5−14] which can find applications for antireflective coatings and microlens structures.[14]

In addition to the electrostatic forces, the particles at a liquid interface may experience also lateral capillary forces due to the overlap of interfacial deformations created by the separate particles.[15−18] For bigger particles (radius >5 μm) the origin of the interfacial deformation can be the particle weight and Archimedes force,[15,16,19] whereas, for submicrometer particles, the deformations of the liquid interface can be due to the particle confinement in a liquid film,[17,18] or to undulated contact line.[3,20−27] For electrically charged particles at a water/nonpolar-fluid interface, another source of interfacial deformation can

*Corresponding author. Phone: (+359) 2-9625310. Fax: (+359) 2-9625643. E-mail: pk@lcpe.uni-sofia.bg.

(1) Binks, B. P.; Horozov, T. S., Eds. *Colloidal Particles at Liquid Interfaces*; Cambridge University Press: Cambridge, UK, 2006.
(2) Kralchevsky, P. A.; Nagayama, K. *Particles at Fluid Interfaces and Membranes*; Elsevier: Amsterdam, 2001.
(3) Kralchevsky, P. A.; Denkov, N. D. *Curr. Opin. Colloid Interface Sci.* **2001**, *6*, 383–401.
(4) Denkov, N. D.; Velev, O. D.; Kralchevsky, P. A.; Ivanov, I. B.; Yoshimura, H.; Nagayama, K. *Langmuir* **1992**, *8*, 3183–3190.
(5) Aveyard, R.; Clint, J. H.; Nees, D.; Paunov, V. N. *Langmuir* **2000**, *16*, 1969–1979.
(6) Aveyard, R.; Binks, B. P.; Clint, J. H.; Fletcher, P. D. I.; Horozov, T. S.; Neumann, B.; Paunov, V. N.; Annesley, J.; Botchway, S. W.; Nees, D.; Parker, A. W.; Ward, A. D.; Burgesset, A. N. *Phys. Rev. Lett.* **2002**, *88*, 246102.
(7) Nikolaides, M. G.; Bausch, A. R.; Hsu, M. F.; Dinsmore, A. D.; Brenner, M. P.; Gay, C.; Weitz, D. A. *Nature* **2002**, *420*, 299–301.
(8) Horozov, T. S.; Aveyard, R.; Clint, J. H.; Binks, B. P. *Langmuir* **2003**, *19*, 2822–2829.
(9) Stancik, E. J.; Kouhkan, M.; Fuller, G. G. *Langmuir* **2004**, *20*, 90–94.
(10) Horozov, T. S.; Aveyard, R.; Binks, B. P.; Clint, J. H. *Langmuir* **2005**, *21*, 407–412.
(11) Horozov, T. S.; Binks, B. P. *Colloids Surf., A* **2005**, *267*, 64–73.
(12) Leunissen, M. E.; van Blaaderen, A.; Hollingsworth, A. D.; Sullivan, M. T.; Chaikin, P. M. *Proc. Natl. Acad. Sci. U.S.A.* **2007**, *104*, 2585–2590.
(13) Leunissen, M. E.; Zwanikken, J.; van Roij, R.; Chaikin, P. M.; van Blaaderen, A. *Phys. Chem. Chem. Phys.* **2007**, *9*, 6405–6414.
(14) Ray, M. A.; Li, J. *Adv. Mater.* **2007**, *19*, 2020–2022.
(15) Nicolson, M. M. *Proc. Cambridge Philos. Soc.* **1949**, *45*, 288–295.
(16) Chan, D. Y. C.; Henry, J. D.; White, L. R. *J. Colloid Interface Sci.* **1981**, *79*, 410–418.
(17) Kralchevsky, P. A.; Paunov, V. N.; Ivanov, I. B.; Nagayama, K. *J. Colloid Interface Sci.* **1992**, *151*, 79–94.
(18) Di Leonardo, R.; Saglimbeni, F.; Ruocco, G. *Phys. Rev. Lett.* **2008**, *100*, 106103.
(19) Paunov, V. N.; Kralchevsky, P. A.; Denkov, N. D.; Nagayama, K. *J. Colloid Interface Sci.* **1993**, *157*, 100–112.
(20) Lucassen, J. *Colloids Surf.* **1992**, *65*, 131–137.
(21) Stamou, D.; Duschl, C.; Johannsmann, D. *Phys. Rev. E* **2000**, *62*, 5263–5272.
(22) Kralchevsky, P. A.; Denkov, N. D.; Danov, K. D. *Langmuir* **2001**, *17*, 7694–7705.
(23) Danov, K. D.; Kralchevsky, P. A.; Naydenov, B. N.; Brenn, G. *J. Colloid Interface Sci.* **2005**, *287*, 121–134.
(24) Loudet, J. C.; Yodh, A. G.; Pouligny, B. *Phys. Rev. Lett.* **2006**, *97*, 018304.
(25) Loudet, J. C.; Pouligny, B. *Europhys. Lett.* **2009**, *85*, 28003.
(26) Lewandowski, E. P.; Bernate, J. A.; Searson, P. C.; Stebe, K. J. *Langmuir* **2008**, *24*, 9302–9307.
(27) Lewandowski, E. P.; Bernate, J. A.; Tseng, A.; Searson, P. C.; Stebe, K. J. *Soft Matter* **2009**, *5*, 886–890.

be the electric field that pushes the particles toward the phase of greater dielectric constant (the water).[7] The nonpolar fluid is usually air or oil. Such deformations have been directly observed and investigated both experimentally and theoretically.[28−30] Furthermore, the overlap of electric-field-induced deformations around two particles may lead to electric-field induced capillary attraction between those that oppose the electrostatic repulsion.[7,31,32] The range of this attractive force is the same as for the electrostatic repulsion, viz., $F \propto 1/L^4$, where L is the distance between the two particles attached to the water/nonpolar-fluid interface.[31,32] The theoretical works[31,32] indicate that, in many cases, the repulsion can dominate the attraction. In such cases, the observed nondensely packed interfacial colloidal crystals[5−14] can be explained by the fact that the particles are enclosed in a restricted space.[33−36] For a topical review, see ref 37.

In recent experiments,[38] we established that electrically charged particles at a water/tetradecane interface experience attractive force, which is stronger than the gravity-induced capillary attraction and prevails over the electrostatic repulsion between the particles. Here, our goal is to find explanation of this effect.

The experiments in ref 38 were carried out with hydrophobized glass spheres of radii in the range $R = 240-320\ \mu$m. When placed at the water/tetradecane boundary, such particles begin to move toward each other under the action of attractive force. Two different procedures of particle hydrophobization were used, which led to obtaining uncharged and charged particles.[38] To establish whether a given particle was charged or uncharged, the meniscus slope angle at the contact line, ψ_c, was measured from side-view photographs of the particles, such as those in Figure 1. For uncharged particles, the experimental angle ψ_c is small and equal to the calculated gravitational angle, ψ_g (see, e.g., Figure 1a). For charged particles, the experimental angle ψ_c is markedly larger than ψ_g (Figure 1b). The reason for working with particle radii of $240-320\ \mu$m is that, for such particles, the angle ψ_c can be measured with good accuracy, which is difficult for smaller particles.

The balance of forces acting on the particle, projected along the vertical z-axis, is

$$F_z^{(g)} + F_z^{(el)} = 2\pi r_c \gamma \sin \psi_c \qquad (1.1)$$

On the left-hand side of eq 1.1, we have the magnitudes of the gravity force, $F_z^{(g)}$, and of the electrodipping force, $F_z^{(el)}$, both of them directed downward (toward the water phase). These two forces are counterbalanced by the vertical resultant of the meniscus capillary force, which is equal to the length of the contact line, $2\pi r_c$, multiplied by the vertical projection of interfacial tension, $\gamma \sin \psi_c$; see the right-hand side of eq 1.1.

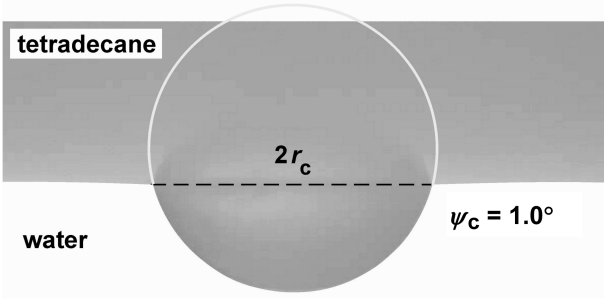

(a) uncharged particle

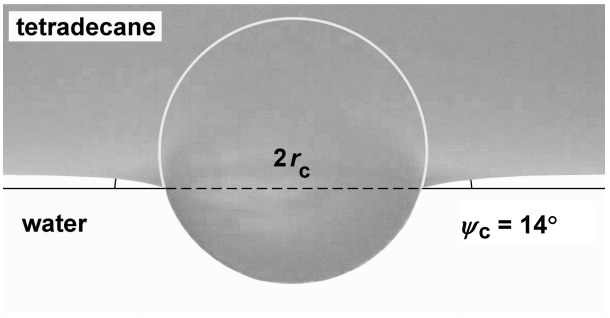

(b) charged particle

Figure 1. Side-view photographs of hydrophobized spherical glass particles at the water/tetradecane boundary. (a) Uncharged particle of radius $R = 283\ \mu$m: the meniscus slope angle due to gravity is relatively small, $\psi_c = \psi_g = 1.0°$. (b) Electrically charged particle of radius $R = 261\ \mu$m: the experimental meniscus slope angle is $\psi_c = 14°$ owing to the electrodipping force. If this force were missing, the gravitational slope angle of the same particle would be only $\psi_g = 0.86°$. The diameter of the contact line, shown dashed in the photos, is denoted as $2r_c$.

$F_z^{(g)}$ is equal to the particle weight minus the Archimedes force and can be calculated from the expression[2]

$$F_z^{(g)} \approx \frac{1}{3}\pi\gamma q^2 R^3 (4D - 2 - 3\cos\alpha + \cos^3\alpha) \quad \text{for} \quad (qR)^2 \ll 1 \qquad (1.2)$$

$$\sin\alpha = \frac{r_c}{R}, \quad D = \frac{\rho_p - \rho_n}{\rho_w - \rho_n}, \quad q^2 = \frac{(\rho_w - \rho_n)g}{\gamma} \qquad (1.3)$$

Here, R is the particle radius; α is central angle; D is a density ratio defined by eq 1.3, where ρ_p, ρ_w, and ρ_n are the mass densities of the particle, water and nonpolar fluid; q^{-1} is the capillary length; g is the acceleration due to gravity; and γ is the interfacial tension of the water/nonpolar-fluid boundary. The angle ψ_g is calculated from eqs 1.1−1.3, where we have set $F_z^{(el)} = 0$ and $\psi_c = \psi_g$.

In section 2, we present new plots of data from ref 38 to demonstrate the additional attraction that is observed in the case of two charged particles. The effect of the menisci formed near the walls of the rectangular experimental cell is also taken into account.

Furthermore, we report data from new experiments aimed at confirming that the electric field of the particles with $\psi_c \gg \psi_g$ is

(28) Danov, K. D.; Kralchevsky, P. A.; Boneva, M. P. *Langmuir* **2004**, *20*, 6139–6151.
(29) Danov, K. D.; Kralchevsky, P. A. *J. Colloid Interface Sci.* **2006**, *298*, 213–231.
(30) Danov, K. D.; Kralchevsky, P. A.; Boneva, M. P. *Langmuir* **2006**, *22*, 2653–2667.
(31) Würger, A.; Foret, L. *J. Phys. Chem. B* **2005**, *109*, 16435–16438.
(32) Oettel, M.; Dominguez, A.; Dietrich, S. *J. Phys.: Condens. Matter* **2005**, *17*, L337–L342.
(33) Hachisu, S.; Kobayashi, Y.; Kose, A. *J. Colloid Interface Sci.* **1973**, *42*, 342–348.
(34) Ohtsuki, T.; Mitaku, S.; Okano, K. *Jpn. J. Appl. Phys.* **1978**, *17*, 627–635.
(35) Pieranski, P. *Phys. Rev. Lett.* **1980**, *45*, 569–572.
(36) Wu, S.; Nikolov, A.; Wasan, D. *Can. J. Chem. Eng.* **2007**, *85*, 562–569.
(37) Oettel, M.; Dietrich, S. *Langmuir* **2008**, *24*, 1425–1441.
(38) Boneva, M. P.; Christov, N. C.; Danov, K. D.; Kralchevsky, P. A. *Phys. Chem. Chem. Phys.* **2007**, *9*, 6371–6384.

really due to surface electric charges, rather than dipoles. To check that, we inserted two electrodes in the form of parallel metal plates in the oily phase. When a particle (with $\psi_c \gg \psi_g$) is present at the liquid interface between the electrodes, it moves toward one of them. These experiments and their interpretation are presented in section 3.

As mentioned above, the additional attraction detected in ref 38 is stronger than the direct electric repulsion between the two like-charged particles and is rather long-ranged. A theoretical model, which can explain the experimental data, is presented in section 4.

2. Comparison of Data for Charged and Uncharged Particles

In ref 38, the center-to-center distance L between two particles at the water/tetradecane interface was recorded as a function of time, i.e., $L = L(t)$ was measured. An illustrative movie showing a record of particle motion toward each other is appended to this article as an electronic Supporting Information file. The purpose of these experiments was to check whether the particle motion is influenced by any electric-field-induced capillary attraction. For this reason, control experiments with uncharged particles were carried out.

As mentioned above, for *uncharged* particles, the meniscus-slope angle at the contact line, $\psi_c = \psi_g$, is small and more difficult for experimental measurement. For this reason, in the experiments with uncharged particles, we used a system of lower interfacial tension, γ, which gives a greater ψ_c at the same particle weight. In these experiments, we used aqueous phase containing 50 mM sodium dodecyl sulfate (SDS) + 50 mM NaCl, for which the interfacial tension against tetradecane is $\gamma = 5.45$ mN/m, and the experimental angle ψ_c varied between 11° and 16° for the investigated particles.[38]

In contrast, for *charged* particles we have $\psi_c \gg \psi_g$, which leads to greater experimental values of ψ_c. However, at large ψ_c we cannot use the theory of capillary forces, which is based on the *linearized* version of Laplace equation for small meniscus slope ($\sin^2 \psi_c \ll 1$). For this reason, in the experiments with charged particles, we used solutions of higher interfacial tension, γ. In these experiments, the aqueous phase contained 0 and 0.1 mM SDS without added NaCl, for which the interfacial tension against tetradecane was, respectively, $\gamma = 52.2$ and 43.8 mN/m, and the experimental angle ψ_c varied between 5.3° and 14.3° for the investigated particles.[38]

Experimental results for uncharged particles are shown in Figure 2 for four pairs of particles. The theoretical fits in Figure 2 are drawn as follows. For uncharged adsorbed particles, the attraction between them can be attributed to the action of the gravity-induced capillary force, which is theoretically described by the expression[16,19,39]

$$F_x = -2\pi\gamma Q_1 Q_2 q K_1(qL) \qquad (2.1)$$

Here, the force F_x is directed along the horizontal x-axis that connects the two particles, and K_1 is the modified Bessel function of the second kind and first order; the coefficients Q_1 and Q_2, called "capillary charges",[19,39] characterize the deformations created by the two particles:

$$Q_1 = r_{c1} \sin \psi_{c1}, \quad Q_2 = r_{c2} \sin \psi_{c2} \qquad (2.2)$$

where r_{c1} and r_{c2} are the radii of the three-phase contact lines on particles 1 and 2; ψ_{c1} and ψ_{c2} are the respective meniscus-slope angles (Figure 1b). In view of eq 1.1 (with $F_z^{(el)} = 0$ for uncharged particles), we obtain

$$Q_i = \frac{F_z^{(g,i)}}{2\pi\gamma} \quad (i = 1, 2) \qquad (2.3)$$

where $F_z^{(g,i)}$ is the vertical gravitational force acting on the ith particle. Using eqs 2.1−2.3, the experimental distance, $L(t)$, was fitted by means of the equation

$$\frac{dL}{dt} = -\frac{2}{\beta_m f_h} F_x, \quad \text{where} \quad F_x = \frac{F_z^{(g,1)} F_z^{(g,2)}}{2\pi\gamma} q K_1(qL) \qquad (2.4)$$

Here, β_m is a mean hydrodynamic resistance, and f_h is a drag coefficient that is given by the Stimson−Jeffrey formula[40] (see eq C.6 in Appendix C, Supporting Information, and eqs 11, 29, and 33 in ref 38). We calculated $F_z^{(g,i)}$ from eq 1.2 for each of the two particles. Then, we fitted the data in Figure 2 by means of eq 2.4 using β_m as a single adjustable parameter. The solid lines in Figure 2 represent the best fits. The excellent agreement between theory and experiment indicates that the attraction between *uncharged* particles is really due to the gravity-induced lateral capillary force. Table 1 shows that the values of β_m determined from the fits in Figure 2 agree well with the respective theoretical values calculated from eq 33 in ref 38. Some differences between the values of β_m determined in the two different ways are due to the hydrodynamic resistance of the meniscus around the particle, which moves together with it.[38] The depth of this meniscus averaged for the two particles, $\bar{h}_g = (h_{g,1} + h_{g,2})/2$, is given in the last column of Table 1. One sees that the difference between the two values of β_m is greater for the larger $\bar{h}_g$ (the theoretical β_m, calculated from eq 33 in ref 38, does not account for the presence of such meniscus).

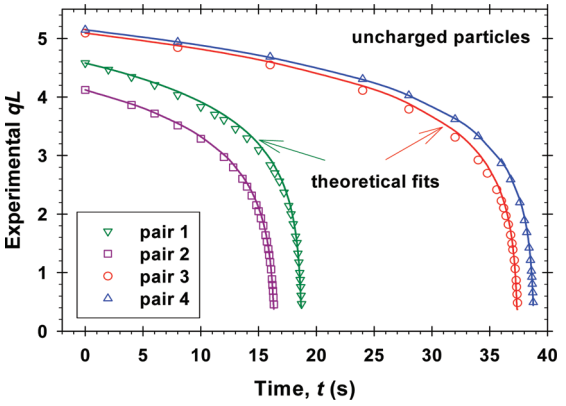

Figure 2. Experimental time-dependences of the interparticle center-to-center distance, $L(t)$, measured for four pairs of uncharged hydrophobic spherical particles attached to the interface between tetradecane and water solution of 50 mM SDS + 50 mM NaCl; the capillary length is $q^{-1} = 1.54$ mm. The data points are from ref 38 and the theoretical fits are drawn by means of eq 2.4.

Table 1. Comparison of β_m Determined from the Fits in Figure 2 and from eq 33 in ref 38

pair no.	β_m (mg/s) from the fit in Figure 2	β_m (mg/s) from eq 33 in ref [38]	$\bar{h}_g$ (mm)
pair 1	14.3	11.6	0.126
pair 2	11.9	10.7	0.101
pair 3	9.92	10.1	0.094
pair 4	11.4	10.2	0.105

(39) Kralchevsky, P. A.; Nagayama, K. *Langmuir* **1994**, *10*, 23–36.

(40) Stimson, M.; Jeffrey, G. B. *Proc. R. Soc. London, A* **1926**, *111*, 110–116.

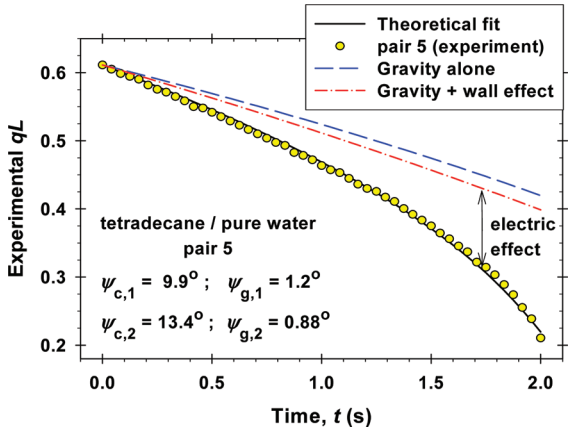

Figure 3. Experimental time-dependence of the interparticle center-to-center distance, $L(t)$, measured for a pair of charged hydrophobic spherical particles attached to the tetradecane/water interface; $\psi_{c,1}$ and $\psi_{c,2}$ are the experimental values of the meniscus slope angle for the two particles, whereas $\psi_{g,1}$ and $\psi_{g,2}$ are the respective calculated values for uncharged particles (gravity force alone). The data points are from ref 38 (pair 5), and the theoretical fit (the solid line) is drawn by means of eq 4.26. The calculated upper long-dash curve shows what would be the distance $L(t)$ if gravity alone were responsible for the particle motion. The dash-dot line was calculated by also taking into account the slight concavity of the interface due to the meniscus on the wall (see the text).

Figure 3 shows a typical set of data from ref 38 for two electrically charged particles, for which $\psi_{c,j} \gg \psi_{g,j}$ (j = 1, 2). To see whether the charge of the particles influences their motion, using eq 2.4 with the theoretical β_m from eq 33 in ref 38, we calculated what would be the distance $L(t)$ if gravity alone were responsible for the particle motion (see the upper long-dash curve in Figure 3). The difference between the latter curve and the experimental points indicates that the charge of the particles leads to acceleration of their motion toward each other. The use of the theoretical β_m in these calculations is justified by the fact that the greatest $\bar{h}_g$ is 0.02 mm in our experiments with charged particles (see Tables 4 and 5 in ref 38), which is about 5 times smaller than $\bar{h}_g$ in Table 1 here. (We recall that, in the experiments with uncharged particles, γ = 5.4 mN/m, whereas, in the experiments with charged particles, $\gamma \geq$ 43.8 mN/m.)

We also took into account the fact that there is a meniscus on the walls of the experimental cell (the water/tetradecane interface does not meet the vertical wall at 90°; see Appendix A, Supporting Information). This leads to the formation of a slightly concave water/tetradecane interface (meniscus). The slope of this meniscus near the center of the cell (where the investigated particles are located) is rather small, but it still could accelerate the particle motion. The dash-dot line in Figure 3 is calculated by taking into account this effect. We see that the influence of the meniscus on the wall on the particle motion is relatively weak, and cannot explain the experimental results (see Appendix A) for details. In our experiments with uncharged particles, the water phase contains 50 mM SDS + 50 mM NaCl. In this case, the capillary length is q^{-1} = 1.54 mm (vs q^{-1} = 4.74 mm for pure water), which leads to a considerably faster decay of the meniscus on the wall. For this reason, the latter effect is neglected when fitting the data in Figure 2.

The data in Figure 3 indicates the action of an additional attraction, which is stronger than the direct electric repulsion between the two like-charged particles. Moreover, this additional attraction is rather long-ranged as compared to the range of the electrostatic meniscus deformations considered in ref 30. We tried various ways to interpret these results. We found only one model, which can explain the experimental data. This model is described in section 4.

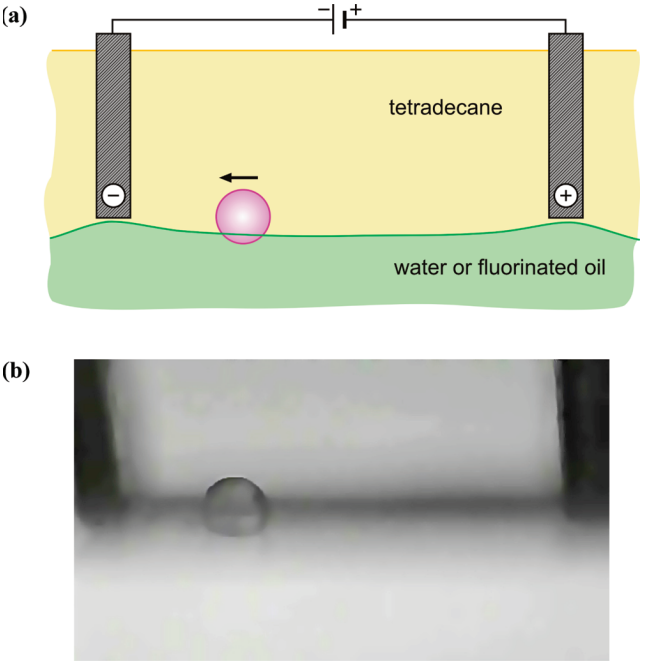

Figure 4. (a) Sketch of a particle located at a liquid interface between two vertical electrodes. The particle is attracted by the cathode and moves toward it. The electrodes are immersed in the upper liquid. Because the lower liquid has a greater dielectric constant, the electric field forms "hills" in the liquid interface just below the electrodes. (b) Photograph of a silanized glass sphere of radius R = 290 μm located at the tetradecane/perfluorocarbon (Flutec LE15) interface between two electrodes.

3. Surface Charges or Surface Dipoles?

3.1. Physical Background. The presence of surface charges at the boundary particle/nonpolar fluid engenders electric field in the nonpolar fluid, which asymptotically behaves as the electric field of a dipole. The reason is the image-charge effect due to the fact that the particle is attached to the water/nonpolar-fluid interface.[5,29] As a result, two similarly charged particles experience a force of electric repulsion, which asymptotically decays as $F_{ER} \propto 1/L^4$ at $L/r_c \gg 1$. Moreover, the particle electric field produces deformation (dimple) in the liquid interface, which decays with the distance as $\zeta \propto 1/r^4$, where r is the radial coordinate. Such profile of the electric-field-induced meniscus around an adsorbed particle has been experimentally confirmed.[30]

However, it can be theoretically proven[8] that an adsorption layer of parallel dipoles at the particle/oil (or particle/air) interface engenders electric field, which asymptotically behaves as the electric field of a dipole. Then, for adsorbed dipoles, the asymptotic behavior of the interaction force and meniscus shape would be similar, viz., $F_{ER} \propto 1/L^4$ and $\zeta \propto 1/r^4$. Then, a question arises: Are the observed phenomena with charged particles at liquid interfaces due to surface charges or surface dipoles?

In an attempt to clarify this issue, we undertook experiments with particles situated between two electrodes. The experimental system is sketched in Figure 4a. The electrodes were two parallel vertical plates immersed in the upper nonpolar fluid, which was tetradecane in our experiments. If the particle has a nonzero net

charge, it would be attracted by one of the electrodes and repelled by the other one. If the particle behaves like a dipole, it would be attracted by each of the electrodes at short distance from it, where the intensity of the electric field is nonuniform.

If the particle is charged, the image-charge effect decreases the effective surface charge, without being able to eliminate it completely. Indeed, the image charge is[41]

$$Q' = -Q\frac{\varepsilon_l - \varepsilon_n}{\varepsilon_l + \varepsilon_n} \quad (3.1)$$

where Q is the original charge (located in the upper fluid), ε_l is the dielectric constant of the lower liquid and ε_n is the dielectric constant of the upper nonpolar fluid. For tetradecane, $\varepsilon_n = 2.0$. If the lower liquid is water with $\varepsilon_l \approx 80$, then the magnitude of Q' is only slightly smaller than $|Q|$. In such case, the image charge strongly decreases the effective net charge, $Q + Q'$ (for $\varepsilon_l > \varepsilon_n$, Q and Q' have opposite signs). To avoid this effect, in some experiments we exchanged the water phase with fluorinated oil. The latter is heavier than tetradecane and is immiscible with it, but has a close dielectric constant. In such case, the magnitude of Q' is markedly smaller than that of Q, and then the reduction of the effective particle charge is smaller.

It should be also noted that eq 3.1 illustrates why any charge Q located in a medium of lower dielectric constant is attracted by the polar phase. Electrostatically, the interaction of the original charge Q with the polar (water) phase is equivalent to the interaction of Q with its mirror image, Q', with respect to phase boundary.[41] (This is the so-called image-charge effect.) Because, for $\varepsilon_l > \varepsilon_n$, Q and Q' have opposite signs (see eq 3.1), this interaction is attraction. This is the reason why charges at the particle/oil interface are attracted by the water phase, and any charges dispersed in air or oil are attracted by the particles (in our experiments the glass particles have dielectric constant $\varepsilon_p = 3.97$).

3.2. Materials. In our experiments we used two kinds of oil phases with different densities: tetradecane and perfluorocarbon fluid. The tetradecane ($C_{14}H_{30}$, for synthesis, Merck) has density $\rho_n = 0.763$ g/cm^3, viscosity $\eta_n = 2.3$ mPa·s and interfacial tension against water 52.2 mN/m. The physical properties of the perfluorocarbon fluid Flutec LE15 (F2 Chemicals, Ltd., UK) are density $\rho_n = 1.7$ g/cm^3, viscosity $\eta_n = 0.656$ mPa·s and interfacial tension against water 11.5 mN/m. The water was purified by a Milli-Q system (Millipore, Inc., USA); its viscosity was $\eta_w = 0.87$ mPa·s. The experiments were carried out at 23 °C.

The used spherical particles were ballotini solid soda glass balls, supplied by Jencons-PLS (UK) with mass density $\rho_p = 2.5$ g/cm^3. The radii of the used particles were in the range between 240 and 320 μm. We hydrophobized the particles by hexamethyldisilazane, $(CH_3)_3SiNHSi(CH_3)_3$ (HMDS, Sigma, USA), using the procedure described in ref 38.

3.3. Experiments. The two electrodes were 1 mm thick rectangular metal plates of dimensions 10 × 100 mm, They were immersed into the upper phase (tetradecane) at a distance 4 mm apart, just above the liquid interface. The voltage applied in our experiments was 60 V DC, which was generated by a stabilized power supply with option for polarity exchange.

The experiments were carried out in a rectangular glass cell (Hellma GmbH & Co., Müllheim, Germany) with inner length, width, and height of 50, 20, and 50 mm, respectively. The motion of the particles was observed by a horizontal optical system and recorded by a CCD camera (SONY XT-ST50CE) connected to a videocassette recorder. The movies were digitized by a video capture board.

First, the two fluids were poured into the cell, and were equilibrated for about 30 min. Then, a particle was placed (through the tetradecane) on the liquid interface between the electrodes, and the voltage was switched on. As a result, we observed that the particle begins to move toward one of the electrodes. The particle does not stick to the electrode, but stops at some distance from it. This distance is greater (about 1 mm) when the lower liquid is water. It is much smaller (about 50 μm) when the lower liquid is fluorinated oil.

This behavior can be explained with the appearance of "hills" on the liquid surface just below the electrodes due to their electric field, which attracts the lower liquid because of its greater dielectric constant. A particle that is climbing such a "hill" stops when the electric and gravitational forces acting on it become equal. When the lower liquid is water (of greater dielectric constant) the "hill" is higher, and the electric force is weaker (due to the image-charge effect). Then, the particle stops at a longer distance from the electrode as compared to the case of fluorinated oil.

After a particle stops, the polarity of the voltage applied to the electrodes is exchanged, and the particle begins to move in the opposite direction, toward the other electrode. Thus, the particle was forced to move between the electrodes many times in the two directions by exchanging the polarity of the electrodes. An illustrative movie showing a record of particle motion in the case of fluorinated-oil substrate is appended to this article as an electronic Supporting Information file.

3.4. Experimental Results and Discussion. The experiments were repeated six times, in different days, with six samples of particles that had been freshly prepared according to the procedure described in ref 38. In five of these experiments, all particles moved toward the cathode, i.e., the particles had positive electric charge. Only in one experiment did all particles move toward the anode, i.e., they were negatively charged.

Different hypotheses about the origin of the surface charge of particles in nonpolar liquids have been discussed: (i) ionization or protonation of polar surface groups, (ii) donor−acceptor interactions involving an electron transfer, and (iii) adsorption of charged ions.[11,42,43] In general, this problem has not yet been solved.

In our experiments, we observed that (i) to obtain charged particles we have to keep the vessel with the dried hydrophobized particles opened for 1 h with free access to atmospheric air; and (ii) in five experiments (in five different days) all particles were positively charged, whereas in one experiment (in another day) all particles were negatively charged. These facts are in agreement with the hypothesis that in our case the particle surface charge can be due to adsorption of ions from the air.

Normal fair-weather ion concentrations are 200−800 negative and 250−1500 positive ions per cubic centimeter of air. The majority of the ions found at or near the surface of the earth are generated by alpha, beta, or γ rays from the natural background radiation. The concentrations of positive and negative ions in air depend on the weather conditions and can vary considerably. Indoor levels are usually lower. Near ground level or in the basement, most positive ions come from radon.[44−47] The ions in

(41) Landau L. D.; Lifshitz, E. M. *Electrodynamics of Continuous Media: Course of Theoretical Physics*; Pergamon Press: Oxford, 1960; Vol. *8*.

(42) Lyklema, J. *Adv. Colloid Interface Sci.* **1968**, *2*, 67–114.
(43) Labib, M. E.; Williams, R. *J. Colloid Interface Sci.* **1987**, *115*, 330–338.
(44) Parts, T.-E. *J. Aerosol Sci.* **1996**, *27*, 445–446.
(45) Nagato, K.; Tanner, D. J.; Friedli, H. R.; Eisele, F. L. *J. Geophys. Res.* **1999**, *104*, 3471–3482.
(46) Hirsikko, A.; Bergman, T.; Laakso, L.; Dal Maso, M.; Riipinen, I.; Hõrrak, U.; Kulmala, M. *Atmos. Chem. Phys.* **2007**, *7*, 201–210.
(47) See "About Air Ions" at http://www.trifield.com/air_ions.htm

air are attracted by the surfaces of solids (of greater dielectric constant) due to the image-charge effect, which facilitates their adsorption.[48] The negative ions are smaller and diffuse faster, which leads to their faster deposition on surfaces. Then, the air remains enriched in positive ions, mostly H_3O^+. This fact and the circumstance that our experiments were carried out in a basement-floor laboratory could explain why the particles were positively charged in most of our experiments. It seems that ions have adsorbed on the surfaces of the dried particles during their 1 h exposition to free contact with atmospheric air. The negative charge of the particles in one of our experiments could be explained with change in the atmospheric conditions that day.

As mentioned above, to obtain charged particles (like that in Figure 1b), we had to keep the vessel with the dried hydrophobized particles opened for 1 h with free access to atmospheric air.[38] When we skipped this step, as a rule we obtained uncharged particles like that in Figure 1a. Hence, in our case, the deposition of charges on the particles happens under specific experimental conditions. Such deposition can be avoided if the experimental procedure is different (e.g., if particle access to atmospheric air is avoided). In other words, the charging of the particles is not a universal phenomenon. Nevertheless, one should have in mind that such electrical effects are possible and may affect the experimental results.

Whatever the origin of the surface charge could be, our experiments with particles between two electrodes indicate that the particles really have nonzero net surface charge. Our next task is to investigate whether or not the electric field of such particles could enhance the capillary attraction between them and explain the results in Figure 3 and other similar data (see the next section).

It should be also noted that the image charge Q', as defined in eq 3.1, is less than Q, in absolute value. Consequently, the particle bears a finite charge, $|Q + Q'| > 0$, and, in the case of a pair of particles, one may expect a charge−charge repulsion, in addition to the dipole−dipole repulsion. This is valid for charged particles at the tetradecane/fluorinated-oil interface. However, in the case of charged particles at the tetradecane/water interface, the situation is more complicated. The electrostatic interaction between the two particles behaves asymptotically as a sum of dipole−dipole repulsion plus *screened* charge−charge repulsion.[37,49,50] Because the Debye screening length in water cannot exceed 1 μm (even in pure water we have 10^{-7} M H^+ and OH^-), the screened charge−charge repulsion quickly decays and becomes negligible at the typical interparticle distances in our experiments with pairs of particles in ref 38.

4. Theoretical Model

4.1. Preliminary Estimates. As already mentioned, the direct electric repulsion between two charged particles attached at the water/nonpolar-fluid interface decays asymptotically as $F_{ER} \propto 1/L^4$ for large L, where L is the interparticle distance.[5,29] This law corresponds to the force-versus-distance dependence between two dipoles. The electric charge is assumed to be located over the particle/nonpolar-fluid interface. Our purpose here is to check whether it is possible to have an electric-field-induced capillary force, which decays more slowly than $1/L^4$ at long interparticle distances. The existence of such force would explain the difference between the experimental data and the dashed theoretical curves in Figure 3.

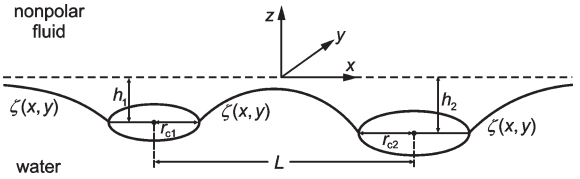

Figure 5. Sketch of the meniscus profile, $z = \zeta(x,y)$, around two charged particles, which are attached to the boundary between a water phase and a nonpolar fluid (air or oil). The contact lines on the particle surfaces are presented by two solid circles of radii r_{c1} and r_{c2}. The distances between the plane of the contact lines and the plane of the nonperturbed interface far from the particles are denoted by h_1 and h_2.

In the estimates of the capillary force, we will use an approach from ref 51. It utilizes the fact that the meniscus slope in the middle between two particles is always small when the interparticle distance L is sufficiently large. Then, the magnitude of capillary force can be expressed in the form[51]

$$F_x = \gamma \int_0^\infty \mathrm{d}y \left[\left(\frac{\partial \zeta}{\partial y}\right)^2 - \left(\frac{\partial \zeta}{\partial x}\right)^2 + q^2\zeta^2 \right]\Bigg|_{x=0} \quad (4.1)$$

Here, $z = \zeta(x,y)$ is the equation of the meniscus shape (Figure 5). In eq 4.1, the integration is over the y-axis, and the integrand must be estimated at the midplane, $x = 0$. Because we assume a small meniscus slope in the midplane, we can use the superposition approximation,

$$\zeta(x,y) = \zeta_1(x,y) + \zeta_2(x,y) \quad (\text{in the midplane } x = 0) \quad (4.2)$$

where ζ_1 and ζ_2 are the menisci created, respectively, by the left- and right-hand-side particle in isolation (in the absence of second particle). Substituting eq 4.2 into eq 4.1, after some transformations we obtain

$$F_x = 2\gamma \int_0^\infty \mathrm{d}y \left(\frac{\partial \zeta_1}{\partial y}\frac{\partial \zeta_2}{\partial y} - \frac{\partial \zeta_1}{\partial x}\frac{\partial \zeta_2}{\partial x} + q^2\zeta_1\zeta_2 \right)\Bigg|_{x=0} \quad (4.3)$$

where we have used the fact that

$$F_x^{(j)} = \gamma \int_0^\infty \mathrm{d}y \left[\left(\frac{\partial \zeta_j}{\partial y}\right)^2 - \left(\frac{\partial \zeta_j}{\partial x}\right)^2 + q^2\zeta_j^2 \right]\Bigg|_{x=0} = 0, \quad j = 1,2 \quad (4.4)$$

In eq 4.4, $F_x^{(1)}$ and $F_x^{(2)}$ are forces acting on the *isolated* particles 1 and 2, and because of that, each of them is equal to zero.

In view of eq 4.3, to estimate the asymptotic behavior of capillary force, one can use the expression

$$F_x \propto \int_{-\infty}^{\infty} \mathrm{d}y \frac{\partial \zeta_1}{\partial y}\frac{\partial \zeta_2}{\partial y}\Bigg|_{x=0} \quad (4.5)$$

For a purely gravitational meniscus, we have $\partial\zeta_i/\partial r \propto K_1(qr) \propto 1/r$, $i = 1,2$, and then eq 4.5 yields $F_x \propto 1/L$, in agreement with eq 2.1. Likewise, for two similar capillary quadrupoles, we have

(48) Danov, K. D.; Kralchevsky, P. A. *Langmuir* **2006**, *22*, 106–115.
(49) Paunov, V. N. *Colloid Polym. Sci.* **2003**, *281*, 701–707.
(50) Park, B. J.; Pantina, J. P.; Furst, E. M.; Oettel, M.; Reynaert, S.; Vermant, J. *Langmuir* **2008**, *24*, 1686–1694.
(51) Velev, O. D.; Denkov, N. D.; Paunov, V. N.; Kralchevsky, P. A.; Nagayama, K. *Langmuir* **1993**, *9*, 3702–3709.

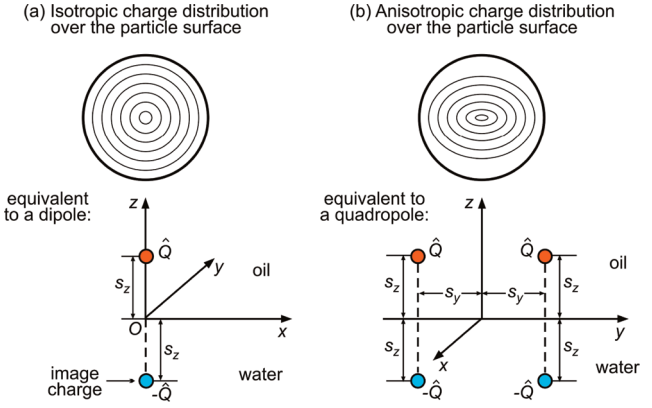

Figure 6. Modeling of the electric field of a charged particle at an oil/water interface. (a) If the distribution of the surface charges is isotropic, the particle can be modeled as a dipole. (b) If the surface-charge distribution is anisotropic, the particle can be modeled as a pair of two parallel dipoles (see the text for details). The distance s_y accounts for the surface-charge anisotropy, whereas s_z accounts for the image-charge effect; $\hat{Q}$ denotes electric charge.

$\partial\zeta_i/\partial r \propto 1/r^3$, $i = 1,2$, and then eq 4.5 yields $F_x \propto 1/L^5$, in agreement with the results in refs 21−23. One could check that the same approach correctly gives the asymptotic behavior of the force between two capillary multipoles of arbitrary order.[23]

As mentioned above, for a particle with *isotropic* distribution of the surface charge (Figure 6a) the particle electric field has asymptotically dipolar character due to the image-charge effect. It was established, both theoretically and experimentally,[30] that, in such a case, $\zeta_1 \propto 1/r^4$, and, consequently, $\partial\zeta_1/\partial r \propto 1/r^5$. Let us assume that the latter interfacial deformation overlaps with the gravitational deformation around the second particle, for which $\partial\zeta_2/\partial r \propto 1/r$. Then, eq 4.5 yields $F_x \propto 1/L^5$. The latter capillary force decays faster than the direct electric repulsion between the two particles, $F_{ER} \propto 1/L^4$. Hence, it cannot explain the experimental results (Figure 3).

Next, let us consider a particle with *anisotropic* distribution of the surface charge (Figure 6b). As a result of the image-charge effect, the electric field of such particle can be modeled as a pair of dipoles directed along the z-axis and separated at a distance $2s_y$. The anisotropy of the particle electric field gives rise to anisotropic electric-field-induced deformation in the liquid interface around the particle, which is equivalent to a capillary quadrupole (see eq 4.23 and eq B.32 in Appendix B, Supporting Information). For a capillary quadrupole, we have $\partial\zeta_1/\partial r \propto 1/r^3$. The latter interfacial deformation overlaps with the gravitational deformation around the second particle, for which $\partial\zeta_2/\partial r \propto 1/r$. Then, eq 4.5 yields $F_x \propto 1/L^3$. The latter capillary force decays slower than the direct electric repulsion between the two particles, $F_{ER} \propto 1/L^4$. Below, we demonstrate that this effect can quantitatively explain the experimental results (see the solid line in Figure 3). The application of eq 4.5 to the particular case of relatively small particles, for which the gravitational deformation is negligible and the whole deformation is only due to the electric field, is considered in Appendix D (Supporting Information).

The existence of surface-charge anisotropy could be explained with the relatively low value of the surface charge density, σ_{pn}, at the particle/nonpolar-fluid interface. Indeed, the average value $\sigma_{pn} \approx 70\ \mu C/m^2$, determined for this type of particles,[28,30] is equivalent to an average distance of 480 Å between two surface charges assuming square packing. At such low average surface density of the adsorbed ions, large fluctuations in their distribution over the particle surface are to be expected. In particular, at a distance of 480 Å, the energy of repulsion between two monovalent ions across oil ($\varepsilon_n = 2$) is only 0.58 kT. Because the binding energy of the ion to the solid surface is expected to be greater, the ion will stay attached to the particle surface at the place where it has first occasionally hit the surface.

4.2. Meniscus Shape around a Particle of Anisotropic Surface Charge Distribution. The potential of the electric field in the nonpolar fluid created by the charge configuration in Figure 6b is

$$\varphi_0 = \frac{\hat{Q}}{\varepsilon_n}[x^2 + (y-s_y)^2 + (z-s_z)^2]^{-1/2} + \frac{\hat{Q}}{\varepsilon_n}[x^2 + (y+s_y)^2 + (z-s_z)^2]^{-1/2} - \frac{\hat{Q}}{\varepsilon_n}[x^2 + (y-s_y)^2 + (z+s_z)^2]^{-1/2} - \frac{\hat{Q}}{\varepsilon_n}[x^2 + (y+s_y)^2 + (z+s_z)^2]^{-1/2} \quad (4.6)$$

where $\hat{Q}$ denotes electric charge; here and hereafter the center of the coordinate system is connected with the considered particle. In ref 30, it was established that the attachment of a charged particle to a liquid interface causes gravitational and electric deformations that are additive with a high precision:

$$\zeta(x,y) \approx \zeta^{(g)}(x,y) + \zeta^{(el)}(x,y) \quad (4.7)$$

where $\zeta^{(g)}$ and $\zeta^{(el)}$ obey the equations (see Appendices A and B):

$$\frac{\partial^2\zeta^{(g)}}{\partial x^2} + \frac{\partial^2\zeta^{(g)}}{\partial y^2} = q^2\zeta^{(g)} \quad (4.8)$$

$$\frac{\partial^2\zeta^{(el)}}{\partial x^2} + \frac{\partial^2\zeta^{(el)}}{\partial y^2} = -\frac{\varepsilon_n}{8\pi\gamma}\left(\frac{\partial\varphi_0}{\partial z}\right)^2\Bigg|_{z=0} \quad (4.9)$$

In Appendix A, it is established that the solution of eq 4.8 for a single particle attached to the meniscus between two fluid phases in an experimental cell of rectangular cross-section is

$$\zeta^{(g)} = -\frac{F_z^{(g)}}{2\pi\gamma}K_0(qr) + h^{(m)}\frac{r_c^2}{r^2}\cos(2\phi) \quad (4.10)$$

Here and hereafter, (r,ϕ) are polar coordinates in the horizontal xy-plane, which coincides with the planar liquid surface far from the particle; the coordinate origin is in the center of the particle contact-line projection on the xy-plane; K_0 is the modified Bessel function of the second kind and zero order; and

$$h^{(m)} \approx \frac{qr_c^2\tan\psi_b}{4\sinh(qb_c/2)} \quad (4.11)$$

where b_c is the width (the length of the shortest side) of the experimental cell, and ψ_b is the meniscus slope angle at the walls of the cell (see eq C.3 in Appendix C). The term with $h^{(m)}$ accounts for the effect of the walls of the experimental cell. This effect disappears when b_c is sufficiently large (see eq 4.11).

Let us consider the deformation in the liquid interface, which is due to the particle's electric field. In terms of the polar coordinates

(r,ϕ), eq 4.9 acquires the form

$$\frac{1}{r}\frac{\partial}{\partial r}\left(r\frac{\partial \zeta^{(el)}}{\partial r}\right) + \frac{1}{r^2}\frac{\partial^2 \zeta^{(el)}}{\partial \phi^2} = -\frac{\varepsilon_n}{8\pi\gamma}\left(\frac{\partial \varphi_0}{\partial z}\right)^2\Bigg|_{z=0} \quad (4.12)$$

The respective boundary conditions are

$$\zeta^{(el)} = -h_c^{(el)} \quad \text{at} \quad r = r_c; \qquad \zeta \to 0 \quad \text{at} \quad r \to \infty \quad (4.13)$$

Here, $h_c^{(el)}$ is the depth of the meniscus at the particle contact line with respect to the level of the flat liquid interface far from the particle. The boundary condition at $r = r_c$ corresponds to fixed contact line at the particle surface. This is a realistic boundary condition, because contact-angle hysteresis is usually present at solid surfaces, the absence of hysteresis being exclusion.[52−58] We will seek the solution of eq 4.12 in the form

$$\zeta^{(el)}(r,\phi) = \xi_0(r) + \xi_2(r)\cos(2\phi) \quad (4.14)$$

From eqs 4.6, 4.12 and 4.14 we obtain the following equations for the coefficient functions (Appendix B):

$$\frac{1}{r}\frac{d}{dr}\left(r\frac{d\xi_0}{dr}\right) = -\frac{\hat{Q}^2 s_z^2}{\pi\gamma\varepsilon_n}\frac{2(r^2 + s_y^2 + s_z^2)^2 + 15 s_y^2 r^2}{(r^2 + s_y^2 + s_z^2)^5} \quad (4.15)$$

$$\frac{1}{r}\frac{d}{dr}\left(r\frac{d\xi_2}{dr}\right) - \frac{4}{r^2}\xi_2 = \frac{\hat{Q}^2 s_z^2}{\pi\gamma\varepsilon_n}\frac{15 s_y^2 r^2}{(r^2 + s_y^2 + s_z^2)^5} \quad (4.16)$$

$$\xi_0(r_c) = -h_c^{(el)}; \quad \xi_2(r_c) = 0; \quad \lim_{r\to\infty}\xi_0(r) = 0; \quad \lim_{r\to\infty}\xi_2(r) = 0 \quad (4.17)$$

The long distance asymptotics of the solution of eq 4.15 is (Appendix B)

$$\xi_0 \approx -\frac{\hat{Q}^2 s_z^2}{8\pi\gamma\varepsilon_n r^4} + \ldots \quad \text{for} \quad r \gg r_c \quad (4.18)$$

Because ξ_0 describes the interfacial deformation produced by isotropic electric field, we have $\xi_0 \propto 1/r^4$, as expected (see above). Furthermore, the general solution of eq 4.16 reads (Appendix B)

$$\xi_2 = A_1 r^2 + \frac{A_2}{r^2} + \frac{5\hat{Q}^2 s_y^2 s_z^2 (3r^2 + s_y^2 + s_z^2)}{32\pi\gamma\varepsilon_n r^2 (r^2 + s_y^2 + s_z^2)^3} \quad (4.19)$$

where A_1 and A_2 are integration constants. From the boundary condition $\xi_2 = 0$ at $r \to \infty$, we obtain $A_1 = 0$. From the boundary condition $\xi_2 = 0$ at $r = r_c$ we obtain

$$A_2 = -\frac{5\hat{Q}^2 s_y^2 s_z^2 (3r_c^2 + s_y^2 + s_z^2)}{32\pi\gamma\varepsilon_n b^6}, \quad b^2 \equiv r_c^2 + s_y^2 + s_z^2 \quad (4.20)$$

The term A_2/r^2 in eq 4.19 is the source of the long-range deformation, $\xi_2 \propto 1/r^2$, created by the four-charge configuration in Figure 6b. This deformation appears because the anisotropic electric field tends to produce a *saddle-shaped* meniscus around the particle, but the *isotropic* boundary condition for fixed contact line, $\xi_2(r_c) = 0$, must be preserved. This leads to a nonzero value of the coefficient A_2 (see eq 4.20). For this reason, the higher-order quadrupolar term ξ_2 (Figure 6b) produces a deformation of longer range ($\xi_2 \propto 1/r^2$) than the dipolar term (Figure 6a), which yields $\xi_0 \propto 1/r^4$ (compare eqs 4.18 and 4.19). The asymptotic form of eq 4.19 is

$$\xi_2 = \frac{A_2}{r^2} + \frac{15\hat{Q}^2 s_z^2 s_y^2}{32\pi\gamma\varepsilon_n}\frac{1}{r^6} + \ldots \quad \text{for} \quad r \gg r_c \quad (4.21)$$

where A_2 is given by eq 4.20.

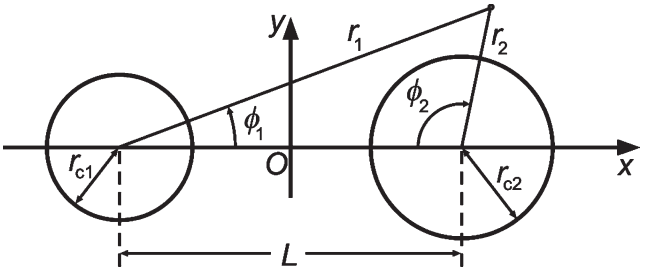

Figure 7. Polar coordinates (r_1,ϕ_1) and (r_2,ϕ_2) in the xy-plane connected with the two particles. The projections of the particle contact lines on the xy-plane are presented by two solid circles of radii r_{c1} and r_{c2}.

4.3. Interaction between Two Particles at a Liquid Interface. Let us consider two particles separated at a center-to-center distance L. In view of eq 4.7, the shape of the meniscus around each particle in isolation can be expressed in the form[30]

$$\zeta_j(x,y) = \zeta_j^{(g)}(x,y) + \zeta_j^{(el)}(x,y), \quad j = 1,2 \quad (4.22)$$

where the subscript j numbers the particles. In general, the multipole expansion of capillary deformation reads

$$\zeta_j(r_j,\phi_j) = \sum_{n=0}^{\infty} A_{j,n} K_n(qr_j)\cos(n\phi_j) \quad (4.22a)$$

where r_j is the length of the position vector with origin in the center of the contact line of the particle j; the angles ϕ_1 and ϕ_2 are shown in Figure 7; q^{-1} is the capillary length; K_n are modified Bessel functions of the second kind; $A_{j,n}$ are coefficients in the expansion. When applying the latter expansion to interpret our set of experimental data, we notice that the data for uncharged particles, described by the term with $n = 0$ in eq 4.22a, correspond to the range $0 < qL < 5$ (Figure 2), whereas the data for charged particles, whose interpretation includes also contributions from terms with $n > 1$, correspond to the range $0 < qL < 0.8$ (Figure 8). For this reason, for $n > 1$ we can use the asymptotic formula $K_n(qr_j) \propto 1/r_j^n$, but, for $n = 0$, we have to keep the original function $K_0(qr_j)$. Thus, combining eqs 4.10, 4.14, 4.18, and 4.20 − 4.22, we obtain (Appendix C)

$$\zeta_j = -\frac{F_z^{(g,j)}}{2\pi\gamma}K_0(qr_j) - (h_j^{(el)} - h_j^{(m)})\frac{r_{cj}^2}{r_j^2}\cos(2\phi_j), \quad j = 1,2 \quad (4.23)$$

where terms on the order of $1/r_j^4$ (and higher order terms) have been neglected; r_{cj} is the contact-line radius; $F_z^{(g,j)}$ is the vertical

(52) Bartell, F. E.; Shepard, J. W. *J. Phys. Chem.* **1953**, *57*, 211–215.
(53) Johnson, R. E., Jr.; Dettre, R. H. In *Surface and Colloid Science*; Matijevič, E., Ed.; Wiley: New York, 1969; Vol. *2*, pp 85−153.
(54) Starov, V. M. *Adv. Colloid Interface Sci.* **1982**, *39*, 147–173.
(55) Marmur, A. *Adv. Colloid Interface Sci.* **1994**, *50*, 121–141.
(56) Marmur, A. *J. Colloid Interface Sci.* **1994**, *168*, 40–46.
(57) Drelich, J.; Miller, J. D.; Good, R. J. *J. Colloid Interface Sci.* **1996**, *179*, 37–50.
(58) Iliev, S. D. *J. Colloid Interface Sci.* **1997**, *194*, 287–300.

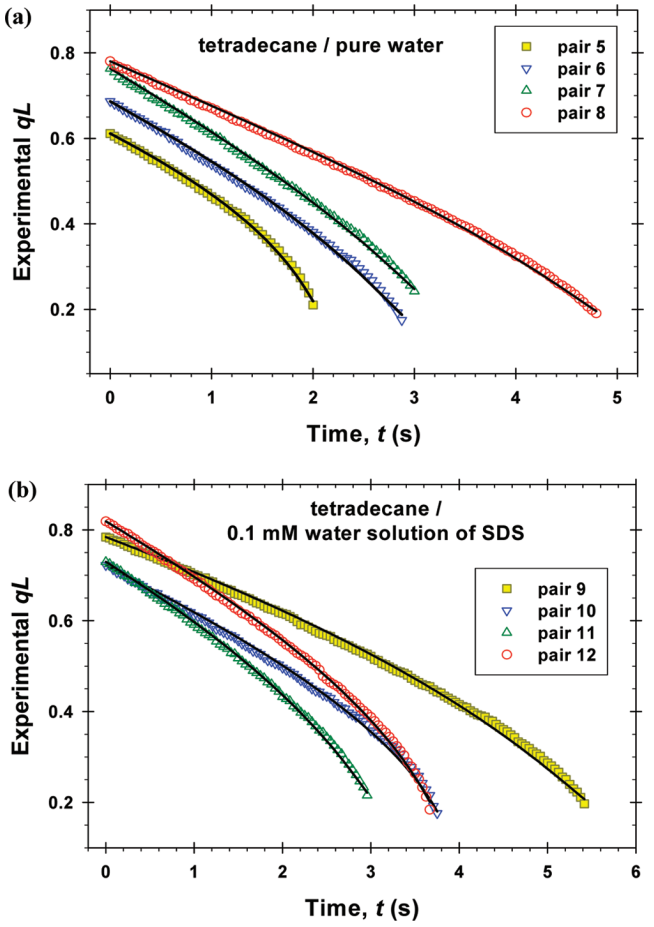

Figure 8. Plots of the dimensionless distance between two particles, qL vs time, t. The experimental points are data from ref 38 with the same numbers of the pairs of particles. The solid lines represent the best fits of the data by means of eq 4.26. (a) The aqueous phase is pure water; $q^{-1} = 4.74$ mm. (b) The aqueous phase is solution of 0.1 mM SDS; $q^{-1} = 4.35$ mm.

gravity force (weight minus Archimedes force) acting on particle j; $h_j^{(m)}$ and $h_j^{(el)}$ are capillary-quadrupole amplitudes defined by eqs 4.11 and B.33 in Appendix B:

$$h_j^{(m)} \approx \frac{qr_{cj}^2 \tan\psi_b}{4\sinh(qb_c/2)}, \quad h_j^{(el)} \equiv \frac{15F_z^{(el,j)}}{32\pi\gamma}\frac{s_{yj}^2}{b_j^2} \tag{4.24}$$

where $F_z^{(el,j)}$ is the electrodipping force acting on particle j, and $b_j^2 \equiv r_{cj}^2 + s_{yj}^2 + s_{zj}^2$. The first term in the right-hand side of eq 4.23 expresses a deformation due to gravity-induced "capillary charge", whereas the second term corresponds to a "capillary quadrupole" (see, e.g., refs 21−23). In particular, $h_j^{(el)}$ is the amplitude of the capillary quadrupole induced by the anisotropic charge distribution on particle surface (Figure 6b). In addition, $h_j^{(m)}$ is the amplitude of the capillary quadrupole induced by the walls of the used rectangular experimental cell. Note that the quadrupolar terms originating from the electric field and from the walls of the cell have the opposite signs. (The numerical results in Table 3 show that, for the investigated system, $h_j^{(m)}$ is much smaller than $h_j^{(el)}$.) Equation 4.24 shows the relation between the parameter of surface charge anisotropy, $s_{y,j}$ and the quadrupole amplitude $h_j^{(el)}$. From the fit of the experimental data, we determined $s_{y,j}/b_j$ as a free adjustable parameter, and then from eq 4.24 we calculated $h_j^{(el)}$ (see below for details).

Next, in view of eq 4.23 we can quantify the force of interaction between the two particles, F_{12}, using expressions derived for the interactions between capillary multipoles of different orders:[23]

$$F_{12} = \frac{F_z^{(g,1)}F_z^{(g,2)}}{2\pi\gamma} qK_1(qL) + F_z^{(g,1)}\frac{2(h_2^{(el)} - h_2^{(m)})r_{c2}^2}{L^3} + F_z^{(g,2)}\frac{2(h_1^{(el)} - h_1^{(m)})r_{c1}^2}{L^3} \tag{4.25}$$

The first term in the right-hand side of eq 4.25 expresses the interaction between the gravity-induced capillary charges of the two particles; the second term is the force between the capillary charge of the first particle and the capillary quadrupole of the second particle; the third term is the force between the capillary charge of the second particle and the capillary quadrupole of the first particle; the force between the capillary quadrupoles of the two particles is $\propto 1/L^5$ and is neglected in eq 4.25 (see Appendix C for details).

The last two terms in eq 4.25 that express the charge-quadrupole interaction are given in their asymptotic form, which deviates by no more than 1.8% from the exact expression in terms of K_n functions in the experimental range $0.2 \le qL \le 0.8$ (see Figure 8 and Appendix E). The error introduced by this approximation in the total force F_{12} does not exceed 0.1% (Appendix E).

It should be also noted that the charge-quadrupole terms in eq 4.25 generally contain a multiplier $\cos(2\phi_j)$, like that in eq 4.23.[23] We have set $\cos(2\phi_j) = -1$, which corresponds to minimal energy, i.e., to the energetically most favorable particle situation, which is spontaneously realized because each particle is free to rotate around a vertical axis. We are assuming that this spontaneous rotation (to the angle of the energy minimum) has been completed before the beginning of our measurements of the interparticle distance L. In the experiments with *charged* particles, we were using an objective of higher magnification to detect more accurately the last stages of particle motion. Initially, we focused on particle 1, and afterward we put particle 2 on the interface. The initial position of particle 2 was out of the microscope observation field. Our measurements of L began when both particles entered the observation field, which corresponds to the last 2−6 s of the experiment, as seen in Figure 8. The whole period of particle motion toward each other was from 30 to 80 s. In other words, the measurements of L were preceded by at least 80% of the period of particle motion. We are assuming that the aforementioned particle rotation has finished during this relatively long preliminary period.

The distance $L(t)$ between the two particles obeys an equation analogous to eq 2.4 (Appendix C):

$$\frac{dL}{dt} = -\frac{2}{\beta_m f_h}\left[F_{12} + \frac{(F_z^{(g,1)} + F_z^{(g,2)})\tan\psi_a}{4\sinh(qa_c/2)} qL\right] \tag{4.26}$$

where F_{12} is given by eq 4.25; the second term in the brackets is the projection of the gravitational force that drives each particle to slide over the concave meniscus due to the wall (see eqs A.16 and A.17 and Figure A.1 in Appendix A); a_c is the long side of the base of the experimental cell; ψ_a is the respective meniscus-slope angle at the wall; β_m is the mean hydrodynamic resistance; and f_h is a drag coefficient calculated using eqs 11 and 33 in ref 38.

4.4. Comparison of Theory and Experiment. The solid lines in Figure 8 represent the best fits of experimental data from ref 38 by means of eq 4.26. The agreement between theory and

Table 2. Hydrodynamic Resistance, β_m, Meniscus Slope Angle, ψ_a, and Dimensionless Anisotropy, s_y/b, of the Surface-Charge Distribution

pair no.[a]	β_m (mg/s)	ψ_a (deg)	s_y/b
Boundary between Tetradecane and Pure Water			
pair 5	7.06	8.83	0.356
pair 6	8.33	6.92	0.201
pair 7	8.39	11.2	0.305
pair 8	7.51	8.99	0.220
Boundary between Tetradecane and 0.1 mM Water Solution of SDS			
pair 9	7.29	2.15	0.200
pair 10	7.17	14.4	0.358
pair 11	7.53	7.01	0.299
pair 12	7.63	11.2	0.294

[a] The numbers of the pairs of particles are the same as those in ref 38.

Table 3. Quadrupolar Amplitudes $h_j^{(el)}$, $j = 1, 2$, and $h^{(m)}$ Induced, Respectively, by the Particle Electric Field and by the Walls of the Rectangular Experimental Cell

pair no.[a]	$h_1^{(el)}$ (μm)	$h_2^{(el)}$ (μm)	$h^{(m)}$ (μm)
Boundary between Tetradecane and Pure Water			
pair 5	5.29	6.11	0.144
pair 6	0.845	1.31	0.134
pair 7	2.24	4.04	0.220
pair 8	1.12	2.62	0.147
Boundary between Tetradecane and 0.1 mM Water Solution of SDS			
pair 9	1.18	1.03	0.029
pair 10	1.77	4.59	0.191
pair 11	1.80	3.35	0.106
pair 12	2.68	3.50	0.168

[a] The numbers of the pairs of particles are the same as those in ref 38.

experiment is excellent. The computational procedure is described in Appendix C. To decrease the number of the adjustable parameters, we have assumed that $\psi_b = \psi_a$ and $s_{y,1}/b_1 = s_{y,2}/b_2 = s_y/b$. Thus, the two adjustable parameters, which have been varied to fit each experimental curve in Figure 8, are ψ_a and s_y/b. All other parameters are known from the experiment. In particular, the electrodipping force in eq 4.24 was calculated from experimentally determined quantities: $F_z^{(el,j)} = 2\pi\gamma r_{cj}(\sin\psi_{c,j} - \sin\psi_{g,j})$, $j = 1, 2$ (see Tables 4 and 5 in ref 38). From the latter two tables and eq 33 in ref 38, we calculated the values of β_m, which are listed in Table 2 here.

In Tables 2 and 3, the numbers of the particle pairs are the same as in ref 38. The values of the adjustable parameter ψ_a and s_y/b determined from the best fit of each experimental curve in Figure 8 are listed in the last two columns of Table 2. The obtained values of ψ_a ($\leq 14.4°$) correspond to small meniscus slope ($\sin^2\psi_a \ll 1$), which is in agreement with the assumptions used in Appendix A to derive the expression for the meniscus shape. The obtained values of s_y/b in the range 0.20−0.36 are reasonable. We recall that $b \equiv (r_c^2 + s_y^2 + s_z^2)^{1/2}$ (Figure 6b), which means that we must really have $s_y/b < 1$.

The existence of surface-charge anisotropy ($s_y/b > 0$) and some differences between the obtained s_y/b values for different pairs of particles (Table 2) could be explained with the relatively low value of the surface charge density, σ_{pn}, at the particle/nonpolar-fluid interface, and with the expected large fluctuation deviations from uniform distribution at such low surface density (see the comment at the end of section 4.1).

In Table 3, we compare the calculated amplitudes of the electric-field induced capillary quadrupoles, $h_1^{(el)}$ and $h_2^{(el)}$, with the average amplitude of the capillary quadrupole induced by the rectangular experimental cell, $h^{(m)}$ (the arithmetic mean of $h_1^{(m)}$ and $h_2^{(m)}$). We see that $h^{(m)}$ is smaller by order of magnitude than $h_1^{(el)}$ and $h_2^{(el)}$. Hence, the capillary quadrupole induced by the rectangular experimental cell is really small and can be neglected. (We took into consideration this term only because initially it was not clear how large the quadrupolar effect due to the cell was.) The main effect of the walls of the experimental cell comes through the second term in the brackets in eq 4.26. This term leads to the difference between the dashed and dash-dotted lines in Figure 3. The latter line is calculated from eq 4.26 setting to zero all electric terms in F_{12} ($h_1^{(el)} = h_2^{(el)} = 0$ in eq 4.25).

The fact that $h^{(m)}$ is negligible in comparison with $h_1^{(el)}$ and $h_2^{(el)}$ allows us to simplify eq 4.25:

$$F_{12} = \frac{F_z^{(g,1)}F_z^{(g,2)}}{2\pi\gamma} qK_1(qL) + 2F_z^{(g,1)}h_2^{(el)}\frac{r_{c2}^2}{L^3} + 2F_z^{(g,2)}h_1^{(el)}\frac{r_{c1}^2}{L^3} \quad (4.27)$$

The last two terms express the interactions between the gravity-induced capillary charges of the two particles with their electric-field-induced capillary quadrupoles. The latter are due to the anisotropy of the surface-charge distribution. The last two terms in eq 4.27 express a hybrid electro-gravity-induced capillary attraction that leads to the experimentally observed faster motion of the particles toward each other (Figure 3). As mentioned above, the last two terms in eq 4.27 are given in their asymptotic form, which is accurate in the experimental range $0.2 \leq qL \leq 0.8$ (see Figure 8 and Appendix E). The more general form of eq 4.27, which is valid for any qL, is[59]

$$F_{12} = \frac{F_z^{(g,1)}F_z^{(g,2)}}{2\pi\gamma} qK_1(qL) + F_z^{(g,1)}qh_2^{(el)}\frac{K_3(qL) + K_1(qL)}{2K_2(qr_{c2})} + F_z^{(g,2)}qh_1^{(el)}\frac{K_3(qL) + K_1(qL)}{2K_2(qr_{c1})} \quad (4.28)$$

Equation 4.27 can be deduced from eq 4.28 with the help of the asymptotic formulas:[60]

$$K_1(x) \approx \frac{1}{x}, \quad K_2(x) \approx \frac{2}{x^2}, \quad K_3(x) \approx \frac{8}{x^3} - \frac{1}{x} \quad \text{for small } x \quad (4.29)$$

Note that the second term in K_3 is canceled by the leading term in K_1, which is the reason for the good accuracy of the approximated eq 4.27.

The values of $h_1^{(el)}$ and $h_2^{(el)}$ in Table 3 are between 0.8 and 5.3 μm, so it turns out that the interfacial quadrupolar deformation could be detected by optical microscopy, by observations of the system from above in reflected light. We did not know in advance what would be the explanation of the experimental curves (like those in Figures 3 and 8). For this reason, all experimental results used in the present paper have been obtained by side-view observations of the particles,[38] which show the meniscus slope angle at the contact line, but cannot show the interfacial deformation related to the capillary quadrupole. The detection of $h^{(el)}$ needs additional experimental investigations, which could be the subject of a subsequent article.

(59) Kralchevsky, P. A.; Danov, K. D. Interactions between particles at a fluid interface. In *Nanoscience: Colloidal and Interfacial Aspects*; Starov, V. M., Ed.; Taylor & Francis: New York, 2009 (in press).

(60) Dwight, H. B. *Tables of Integrals and Other Mathematical Data*, 4th ed.; Macmillan Company: New York, 1964.

5. Summary and Conclusions

In a previous study,[38] we established that the attraction between electrically charged particles attached to a water/tetradecane interface is stronger than predicted on the basis of the gravity-induced lateral capillary force. In the present paper, our goal was to explain this effect. The investigated particles were hydrophobized glass spheres of radii between 240 and 320 μm. Their weight is large enough to deform the liquid interface. The interfacial deformation is considerably greater for charged particles (Figure 1) because of the electrodipping force. The experimental data for uncharged particles agree very well with the theory based on the gravity-induced capillary force (Figure 2). However, this force alone cannot explain the faster motion of charged particles toward each other (Figure 3). By independent experiments with particles placed between two electrodes, we confirmed the presence of electric charges at the particle/tetradecane interface (see 3 and Figure 4). The theoretical analysis shows that, if the distribution of these surface charges is isotropic (Figure 6a), the meniscus produced by the particle electric field decays too fast with distance and cannot explain the experimental observations. However, if the surface-charge distribution is anisotropic (Figure 6b), it induces a saddle-shaped deformation in the liquid interface around the particle. This deformation, which is equivalent to a capillary quadrupole,[21−23] decays relatively slow. Its interference with the gravity-induced isotropic meniscus around the other particle gives rise to a long-range capillary attraction, $F \sim 1/L^3$ (see eq 4.27). The obtained excellent agreement between the experimental and theoretical curves in Figure 8, and the reasonable values of the parameters determined from the fits (Table 2) indicate that the observed strong attraction in the investigated system can be really explained as a hybrid interaction between gravity-induced capillary charges and electric-field-induced capillary quadrupoles (see the last two terms in eq 4.27).

Acknowledgment. This study was supported in part by project DO-02-82/2008 of the National Science Fund of Bulgaria (National Centre for New Materials UNION), and in part by the EU COST Action D43 "Colloid and Interface Chemistry for Nanotechnology". The authors thank Ms. Mariana Paraskova for her assistance in the figure preparation.

Supporting Information Available: Effect of the meniscus due to the walls of the experimental cell (Appendix A); effect of particle electric field on the meniscus shape (Appendix B); particle motion equation and procedure for data processing (Appendix C); application of eq 4.5 to purely electric interfacial deformations (Appendix D); and accuracy of the expression for the interaction force (Appendix E). Movies of the motion of two particles toward each other under the action of capillary attraction (Figure 2) and the motion of a particle between two electrodes (Figure 4b). This material is available free of charge via the Internet at http://pubs.acs.org.